Physical Realizations of Multidimensional Voronoi Constellations in Optical Communication Systems

Citation for the original published paper (version of record):
Mirani, A., Vijayan, K., Li, S. et al (2023). Physical Realizations of Multidimensional Voronoi Constellations in Optical Communication
Systems. Journal of Lightwave Technology, 41(17): 5557-5563.
http://dx.doi.org/10.1109/JLT.2023.3264927

Physical Realizations of Multidimensional Voronoi Constellations in Optical Communication Systems

Ali Mirani, Kovendhan Vijayan, Shen Li, Zonglong He, Erik Agrell, Jochen Schröder, Peter Andrekson, and Magnus Karlsson

***Abstract*—Multidimensional geometric shaping has been shown to outperform uniform quadrature amplitude modulation (QAM) in optical communication systems but the complexity of symbol decision and bit mapping can often be significant as dimensionality increases. In this paper, a low-complexity geometric shaping method based on multidimensional lattices is investigated both in experiments and simulations. The modulation formats designed based on this method are called Voronoi constellations (VCs) and we study them in 8, 16, and 32 dimensions. We obtain transmission reach improvements of up to 22 and 70% for VCs compared to 4QAM and 16QAM, respectively, in nonlinear long-haul fiber transmission. Moreover, we compare different physical realizations of multidimensional VCs over wavelengths, polarizations, and time slots in both the Gaussian and nonlinear fiber channels. We demonstrate that different physical realizations perform similarly in the fiber-optic back-to-back channel. However, in long-haul transmission systems, spreading the dimensions over time slots can increase the transmission reach up to 4% compared to wavelengths and polarizations. Furthermore, the mutual information and generalized mutual information are estimated and compared to QAM formats at the same spectral efficiencies.**

***Index Terms*—Optical communication, multidimensional modulation format, geometric shaping, lattice, Voronoi constellations.**

I. Introduction

GEOMETRIC constellation shaping has become attractive in communication systems due to its flexible design for different impairments [1], e.g., tolerance to laser phase noise [2], [3], fiber Kerr nonlinearities [4]–[6], transceiver components impairments [7], and low signal-to-noise ratio (SNR) channels [8]. In contrast to probabilistic constellation shaping (PCS) [9], [10], geometric constellation shaping (GCS) modifies the Euclidean geometry of the constellation points while keeping their occurrence probability uniform [11], [12, Ch. 4]. Often, these constellation shaping methods are optimized in 2-dimensional (2D) space and they are independently realized over the physical dimensions of optical fibers. For example, in [13], PCS and GCS are compared separately and in a hybrid combination in a 2D Gaussian-noise channel. In [14], an autoencoder-based geometric shaping method is applied in a 2D space in the presence of transceiver impairments.

However, multidimensional GCS has the advantage of optimizing the constellations in the multidimensional Euclidean space with higher degrees of freedom [15], [16] compared to PCS and 2D GCS at the expense of increased design complexity. For example, in [17], an 8-dimensional biorthogonal modulation format was realized over 2 polarizations and 2 wavelengths with 84% transmission reach improvement compared to quadrature phase-shift keying (QPSK) at the same symbol rate but half the bit rate. In [18], a 24-dimensional extended Golay-coded modulation format was realized over polarizations and time slots providing 15% transmission reach improvements compared to dual-polarization binary phase shift keying.

Recently, many efforts have been made to reduce the design complexity for multidimensional constellations [19]. Orthant symmetry [20] and amplitude coding [21] are examples of recent works to reduce the complexity of GCS in 4-dimensional space. Another approach to reduce complexity is the lattice-based modulation named Voronoi constellations (VCs) [22]–[24]. The VCs are shown to be efficient at relatively high SNRs with modulation and demodulation complexity independent of their spectral efficiencies (SEs) [25], [26]. Moreover, no look-up table is required to store the constellation points of VCs, which makes the complexity independent of the constellation size (cardinality). These properties make VCs a suitable option for applications with strict limits on latency or power consumption, e.g., video conferencing or instrument control links that are latency sensitive [25]. The VCs have been realized in optical communication systems at 8 dimensions over time slots [27] and 32 dimensions over multiple wavelengths, polarizations and time slots [28]. Another type of VCs based on cubic coding lattice is investigated in [29] for single and multi-wavelength transmission simulations and mutual information (MI), generalized mutual information (GMI), and bit-error rate (BER) metrics are compared with quadrature amplitude modulation (QAM) formats. However, different physical realizations of VCs over different fiber dimensions have not been compared with each other in optical communication systems.

Conventionally, in communication theory, all signaling dimensions are equal and independent, but in physical realizations, this may not always be the case. For example,

This work was supported by the Knut and Alice Wallenberg Foundation under grant No. 2018.0090, and the Swedish Research Council (VR) under grant No. 2017-03702, 2019-04078, and 2021-03709.

A. Mirani, K. Vijayan, Z. He, J. Schröder, P. Andrekson, and M. Karlsson are with the Department of Microtechnology and Nanoscience, Chalmers University of Technology, SE-41296 Gothenburg, Sweden (email: mirani@chalmers.se; vijayan@chalmers.se; zonglong@chalmers.se; jochen.schroeder@chalmers.se; peter.andrekson@chalmers.se; magnus.karlsson@chalmers.se).

S. Li, and E. Agrell are with the Department of Electrical Engineering, Chalmers University of Technology, SE-41296 Gothenburg, Sweden (email: shenl@chalmers.se; agrell@chalmers.se).

in a quantum-noise limited channel, a single quadrature in a polarization component cannot be detected or exchanged without incurring a penalty or exchange of the other quadrature (which is fundamentally originating from Heisenberg's uncertainty relation and the photon no-cloning theorem) [30], [31]. This is in contrast with polarization components that can be losslessly separated and processed individually. Another example, of more relevance for this work, is the nonlinear fiber channel, where it is unclear and not systematically investigated whether the nonlinear distortions will affect polarization/quadrature/time/wavelength dimensions equally or not.

In this paper, which is an extension of [27] and [28], we investigate different realizations of VCs in 8, 16, and 32 dimensions and compare their BER performance both in simulation and experiment in back-to-back (B2B) and long-haul fiber transmission. We show up to 22 and 70% transmission reach improvement for VCs compared to 4QAM and 16QAM at the hard-decision forward error correction (HD-FEC) limit, respectively. Moreover, we show that spreading the VCs dimensions over time slots rather than wavelengths and polarizations can provide slightly higher transmission reach, up to 4% at the HD-FEC limit. Furthermore, the MI and GMI are estimated for some of these VCs to show the achievable gains when they are combined with multilevel coding (MLC) and bit-interleaved coded modulation (BICM) schemes.

The remainder of the paper is organized as follows. In section II, we describe the VCs and their physical realizations in optical fiber transmission systems. In section III, we present simulation results for the multidimensional additive white Gaussian noise (AWGN) channel and nonlinear fiber transmission using the split-step Fourier method (SSFM). In section IV, the experimental results for B2B and long-haul transmission by a recirculating loop are demonstrated. Finally, the conclusion of this paper is presented in Section V.

II. Voronoi Constellations and Physical Realizations

A VC is a set of multidimensional vectors based on two lattices, viz. a shaping lattice and a coding lattice. The outer boundary of the constellation is determined by the scaled Voronoi region of the shaping lattice, and the constellation points are selected from the coding lattice vectors inside this boundary [28]. For example, QAM formats are generated using integer (cubic) lattices for both the shaping and coding lattices, providing 0 dB shaping and coding gains [26]. Therefore, QAM formats are usually used as a benchmark to compare the performance of other modulation schemes.

The VCs covered in this paper are based on the 8-dimensional Gosset lattice (E8), and the 16- and 32-dimensional Barnes–Wall lattices (BW16 and BW32, respectively) [32, Ch. 4], [33] with SEs β of 1 and 2 bits/sym/dimension. These modulation formats are named as E8B1, E8B2, BW16B1, BW16B2, BW32B1, and BW32B2, having 256, 65536, 65536, $\sim 4.3\times10^{9}$, $\sim 4.3\times10^{9}$, and $\sim 1.8\times10^{19}$ constellation points, respectively. The modulation (bits to transmitted symbol mapping) and demodulation (received symbol to bits demapping) of VCs are discussed in detail in [25].

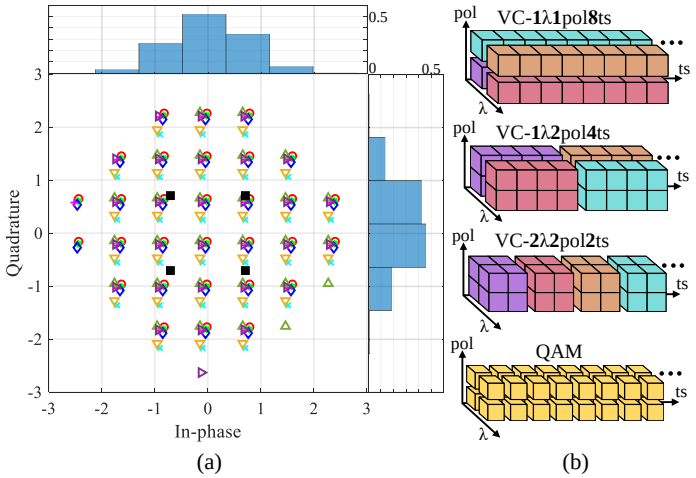

Fig. 1: (a) 2D projection of the BW16B1 constellation with a unit average energy. Each marker and color corresponds to a pair of dimensions. The bars on the top and right show the histogram of the constellation points. The black square marker shows the 4QAM format at the same SE with unit energy. (b) Investigated physical dimensions in a single-mode fiber to transmit 16D symbols (colorized). Each small cube represents a 2D symbol. QAM formats with independent symbols are shown at the bottom as separate cubes.

To transmit a multidimensional VC over physical fiber dimensions, we convert the multidimensional symbol into multiple 2D symbols to modulate the amplitude and phase, i.e., in-phase and quadrature (IQ) components, in different combinations of time slots (ts), polarizations (pol), or wavelengths (λ). The spatial dimensions (multi-core and multi-mode fibers) [34], [35] offer additional degrees of freedom, which are not covered in this paper. An example of a 2D projection of the BW16B1 format is shown in Fig. 1 (a) together with 4QAM at the same SE and unit energy. It is evident that a multidimensional VC has a bell-shaped probability distribution in the 2D projection, which approximates a Gaussian distribution, i.e., the optimum input distribution for the AWGN channel. Moreover, we observe that the VC has more levels and higher expansion in 2D space [24] compared to the equivalent QAM format, which can potentially degrade the performance of the VC in the presence of high transmitter noise or nonlinearity.

In Fig. 1 (b), we show examples of possible physical realizations of a 16-dimensional (16D) modulation format given our hardware limitations in the lab, i.e., 2 wavelengths with dual-polarization transmitters. In Fig. 1 (b), from top to bottom, we expand the modulation format dimensions from time slots to polarization and wavelengths. First, each 16D symbol is realized over 1 wavelength, 1 polarization, and 8 time slots. Then, each symbol is realized over 1 wavelength, 2 polarizations, and 4 time slots. Finally, each 16D symbol is implemented over 2 wavelengths, 2 polarizations, and 2 time slots. The same concept can be generalized if more wavelengths are available or spatial dimensions are added in multi-core or multi-mode fiber systems. It should be mentioned that each time slot carries two dimensions in each polarization

and wavelength, i.e., IQ components. The QAM formats are shown with independent cubes in every time slot, polarization, and wavelength with independent IQ components. These realizations of physical dimensions all yield the same bit rate at a given bandwidth, i.e., the same SE.

To transmit the 16QAM and VCs payload symbols in our experimental setup, we use the pilot-based frame structure described in [36], [37] for each polarization and wavelength. Blind digital signal processing (DSP) has been used for the checkerboard (D_4) lattice previously in [38], [39], but a pilot-based DSP is easier and more flexible. The frame consists of an initial sequence of 4QAM symbols for frame synchronization and pilot-based equalization followed by a payload sequence. The payload can be any higher-order QAM formats or VCs, which are realized in 2D according to Fig. 1 (b). The total frame length is 2^{16} time slots, and the initial pilot length is 2^{12} time slots. For every 31 time slots in the payload sequence, one 4QAM pilot is inserted for phase noise compensation. This corresponds to an overall pilot overhead of approximately 9.2% in a frame. The pilot overhead can be optimized to maximize the throughput of the system [37]. Unlike 16QAM and VCs, 4QAM payloads are transmitted without pilots, and blind algorithms are used at the receiver.

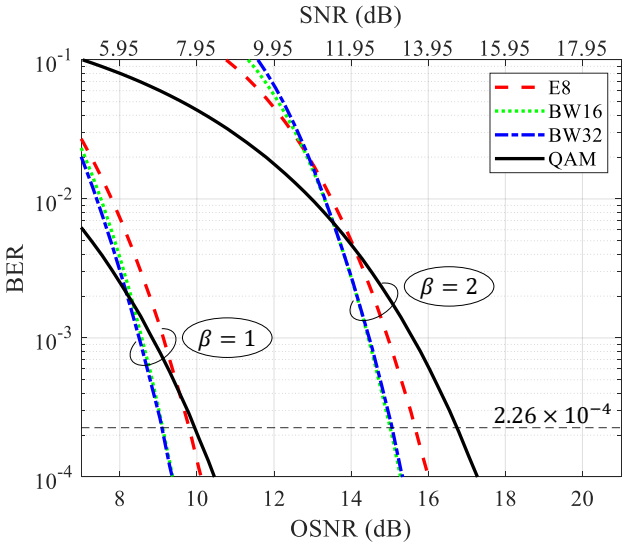

Fig. 2: The BER simulation of VCs and QAM formats vs the OSNR and SNR per dimension at 20 GBaud over the multidimensional AWGN channel. QAM formats are labeled by Gray mapping and VCs are quasi-Gray mapped based on [25].

III. Simulation Results

The performance of VCs is investigated over the AWGN channel and long-haul nonlinear fiber channel without transceiver implementation penalties. We study the performance metrics of MI, GMI, and BER; however, because of the lower computational complexity, we focus mostly on BER in this paper.

A. BER estimation

The uncoded BER metric can be easily calculated by comparing the transmitted and received bits. In Fig. 2, we show the BER performance of VCs over a zero-mean multidimensional AWGN channel $\mathcal{N}(\mathbf{0}, \frac{N_0}{2}\mathbf{I}_{N\times N})$, where $\mathbf{I}$ is the identity matrix, N is the dimensionality, and $N_0/2$ is the variance of the Gaussian noise in each dimension. The SNR per dimension is $SNR = E_s/(N \cdot N_0/2)$, where E_s is the average energy of the constellation. The optical signal-to-noise ratio (OSNR) is $OSNR = SNR \cdot R_s/B_n$ assuming an amplified spontaneous emission (ASE) noise-limited optical channel, where B_n is the optical noise bandwidth equivalent to 0.1 nm, and R_s is the 2D symbol rate 20 GBaud.

Fig. 2 shows that below a certain BER at the crossing points of the curves, the VCs outperform the uniform QAM at the same SE. The OSNR improvements at lower BERs are due to the power-efficient design of VCs in higher dimensions [25]. At the HD-FEC limit of $BER = 2.26 \times 10^{-4}$, which applies to the KP4 code [40], the OSNR improvements are approximately 0.14, 0.84, and 0.85 dB at $\beta = 1$ bits/sym/dimension, and 1.08, 1.68, and 1.73 dB at $\beta = 2$ bits/sym/dimension for E8, BW16, and BW32 compared to QAM, respectively. However, at high BERs, the QAM formats have a better performance due to a lower kissing number [32, Ch. 1] and efficient Gray labeling. Therefore, it can be concluded that VCs are a better option for high-SNR applications compared to QAM formats. Moreover, we see that VCs based on the BW16 lattice can perform similarly to the BW32 [27] with a lower complexity.

In Fig. 3, we show the simulation results for the VCs and QAM formats by solving the Manakov model [41] using the SSFM [42, Ch. 2] in a long-haul transmission link for a two-wavelength and dual-polarization system. The fiber is modeled with 0.2 dB/km attenuation, 16.8 ps/nm/km dispersion, and 1.3 (W km)$^{-1}$ nonlinearity. Each span of fiber is 80 km and it is followed by an erbium-doped fiber amplifier (EDFA) with 5 dB noise figure and a gain equivalent to the span loss, i.e., 16 dB. The dispersion is only compensated at the receiver side, and the optical launch power is optimized to achieve the lowest BER. The BER is averaged over independent symbols, which are realized over the physical dimensions of the fiber channel.

Fig. 3 shows a comparison of different physical realizations of VCs with each other and with the QAM formats at the same SE. In each subfigure of Fig. 3, at low BERs and short transmission distances, all VCs and their physical realizations outperform uniform QAM. At the HD-FEC limit of $BER = 2.26 \times 10^{-4}$, the transmission distance improvements are approximately 1.2, 14.1, and 15.4% at $\beta = 1$ bits/sym/dimension, and 5.8, 15.6, and 19.0% at $\beta = 2$ bits/sym/dimension for E8, BW16, and BW32 compared to QAM, respectively. However, at long transmission distances, the QAM formats outperform the VCs with the same SEs. Furthermore, among different physical realizations of VCs, it is shown that spreading the dimensions over time slots and using independent VCs on each wavelength and polarization provides a slightly higher transmission reach.

These observations are consistent with [43], [44], where

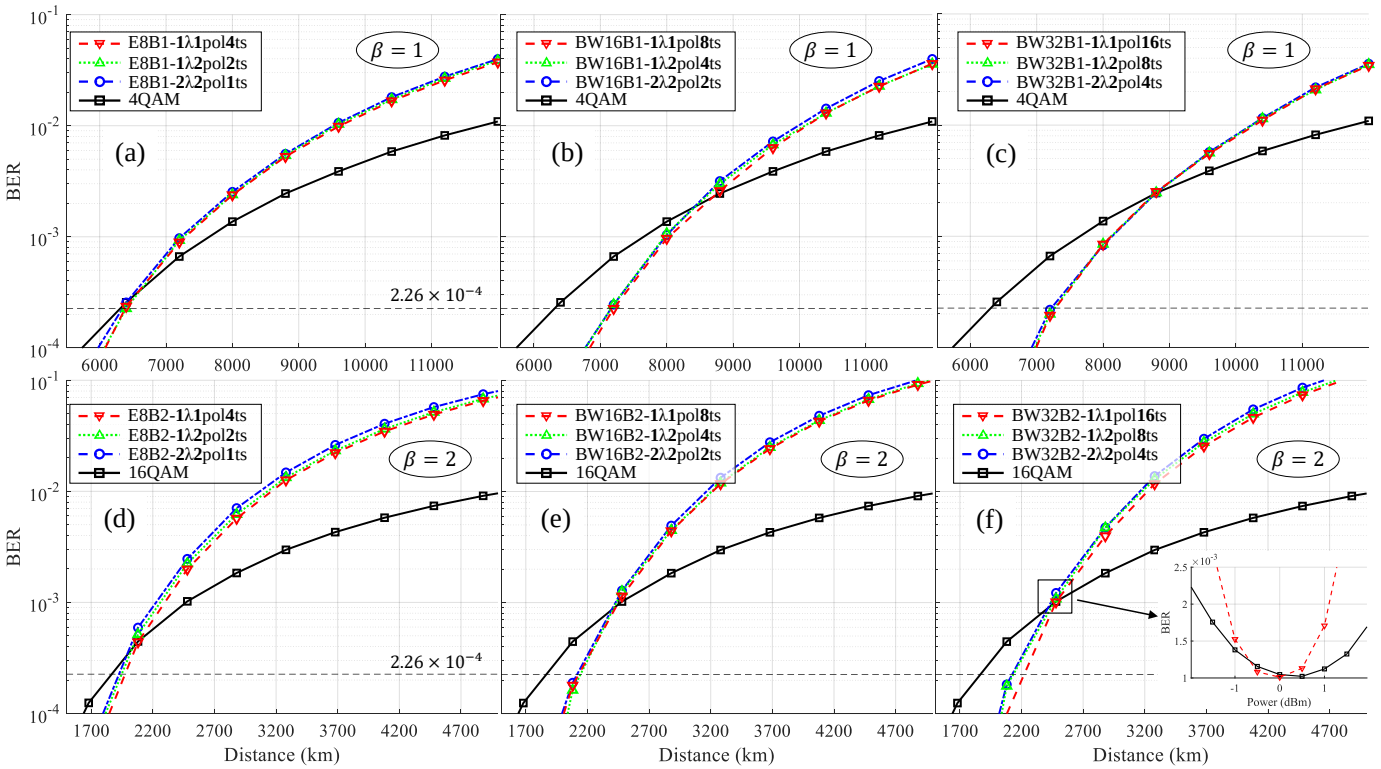

Fig. 3: BER simulation of VCs with different physical realizations and QAM formats using the SSFM. The performance is shown at the optimum optical launch power. The inset shows BER vs. optical power at a specific transmission distance.

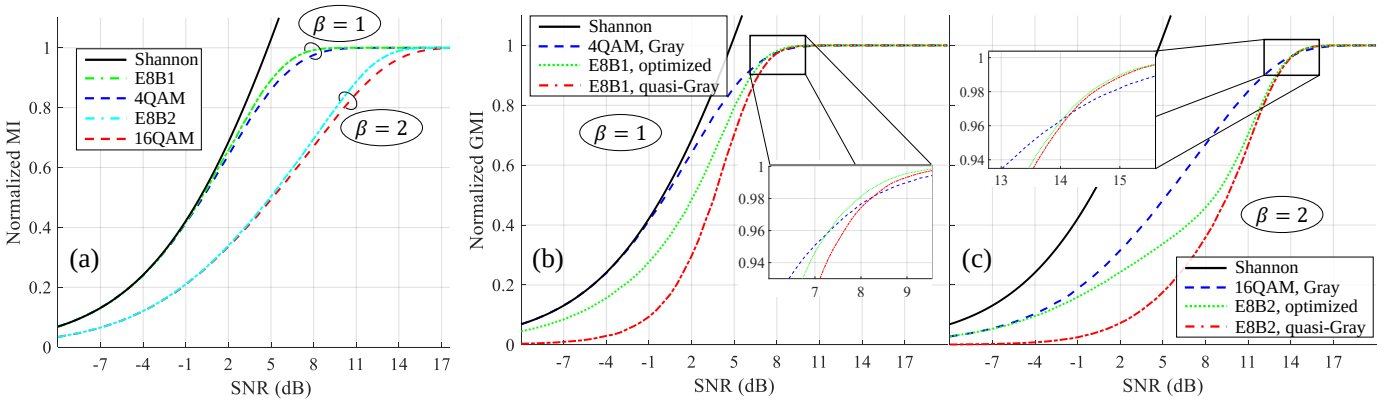

Fig. 4: (a) Normalized MI vs. SNR per dimension for VCs based on E8 lattice and QAM formats over the multidimensional AWGN channel. (b) and (c) Normalized GMI performance with different labelings. The insets show the regions where VCs outperform QAM formats.

4-dimensional formats showed very similar performance for different physical realization strategies. In this work, the better performance of the time slot realization might be due to our usage of disjoint DSP in the receiver for different polarizations and wavelengths, which results in a similar noise distribution among constellation dimensions when VCs are spread only over time slots.

B. MI and GMI estimation

Better metrics to predict the performance of modulation formats combined with soft-decision forward error correction (SD-FEC) are MI and GMI [45]. Generally, estimating MI and GMI accurately is time-consuming for VCs since their cardinality can be extremely high [25], [33]. Recently, the MI and GMI for VCs with a cubic coding lattice have been approximated [29], [46] based on importance sampling [33]. In this section, we estimate the MI and GMI for two E8-based constellations with moderate cardinalities (256 and 65536 constellation points) based on Monte Carlo simulations.

In Fig. 4 (a), we show the normalized MI performance over a zero-mean multidimensional AWGN channel. The normalized MI is estimated using [47, Eq. (21)] divided by

the number of bits per symbol βN. In Fig. 4 (a), in both SEs, the VCs based on the E8 lattice outperform the QAM formats due to their shaping gain and constellation power efficiencies [25]. This shows the achievable SNR gains by designing an MLC scheme for VCs compared with QAM formats.

In Fig. 4 (b) and (c), the normalized GMI performance, i.e., the GMI [47, Eq. (22)] divided by the number of bits per symbol βN, of VCs based on the E8 lattice and QAM formats are shown for $\beta = 1$ and 2 bits/sym/dimension, respectively. For QAM formats, Gray labeling is used, and for VCs, a quasi-Gray labeling [25] and an optimized labeling based on [48] and [8] are applied. Based on the normalized GMI performance in Fig. 4 (b) and (c), the QAM formats outperform VCs except at high SNRs, which are shown in the insets. This is due to lower kissing number [32, Ch. 1] and efficient Gray labeling for QAM formats compared to VCs. However, at very high SNRs, because of the power efficiency of VCs, they outperform QAM formats. This shows that for bit-interleaved coded modulation schemes with the typical forward error correction (FEC) overheads of around 20%, the QAM formats are a better option than VCs.

IV. Experimental Results

To verify the simulation results, we experimentally realize the VCs and QAM formats for a B2B and long-haul transmission experiment using a recirculating loop. The experimental setup is shown in Fig. 5 (a). The performance is evaluated in terms of the pre-FEC BER, which as discussed in Sec. III-A is the relevant metric for HD-FEC systems. The experimental verifications of VCs in SD-FEC systems, where the MI and GMI are relevant metrics, remains for future work.

At the transmitter side, optical carriers are generated from two independent external cavity lasers of linewidths $\leq$100 kHz operating at 1550.12 and 1550.32 nm, i.e., $\sim$25 GHz spacing. Each laser is split up into two arms by a 3 dB coupler and modulated by an IQ modulator driven by 20 Gbaud amplified electrical signals from an arbitrary waveform generator (AWG) with 8 bits vertical resolution. A higher symbol rate will induce higher implementation penalties and might increase the transmission nonlinearities for VCs compared to QAM formats; however, investigation of symbol rate effects remains for future works. A variable optical attenuator (VOA) after each modulator is used to balance the power of the arms with respect to other arms. For each wavelength, the output of the VOAs are combined using a polarization beam combiner to create a dual-polarization signal. Finally, the two wavelengths are combined using a 3 dB coupler. Nonlinear interference from copropagating wavelength channels could be emulated by adding shaped ASE noise at this stage, which is however not studied in this work.

The optical channel includes a VOA to sweep the OSNR and a recirculating loop. The recirculating loop consists of acousto-optic modulators (AOMs), a 3 dB coupler, an EDFA to compensate for the loop losses (losses in the wavelength selective switch (WSS), AOM, and 3 dB coupler), a loop-synchronized polarization scrambler, two stages of optical bandpass filters

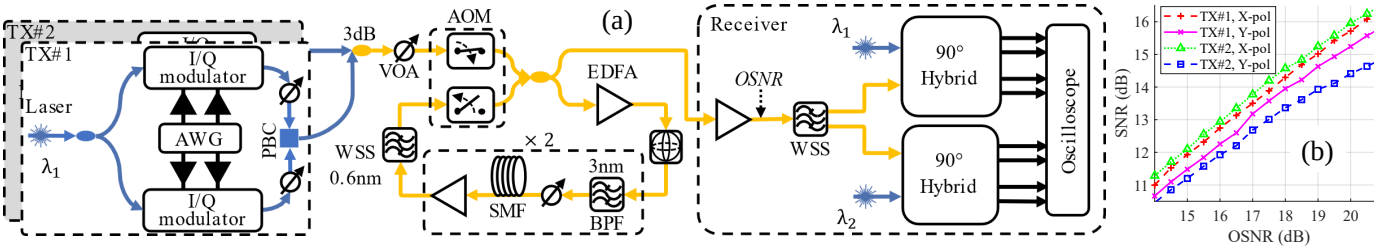

Fig. 5: (a) The setup for the 2 wavelengths and 2 polarizations in the B2B and recirculating loop experiments, (b) Normalized SNR performance for each IQ component in the B2B setup with 16QAM payloads.

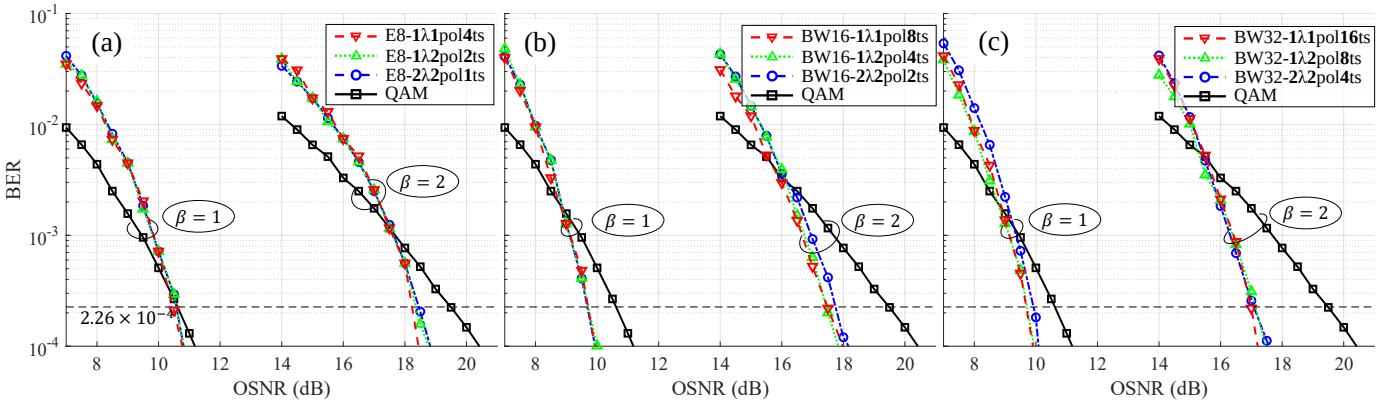

Fig. 6: Experimental BER performance vs. the measured OSNR in the B2B setup. The OSNR is measured over 2 wavelengths and 2 polarizations with 0.5 nm bandwidth resolution and it is normalized per dimension and 0.1 nm noise bandwidth.

(BPFs) to remove the out-of-band ASE noise, VOAs to set the launch power into approximately 80 km standard single-mode fiber (SMF) spans, EDFAs to compensate for span losses at a constant gain of 30 dB, and a WSS to equalize the gain-tilt of the EDFAs. The mismatch between the amplifier gains and the span losses is due to the limited configuration setting of the amplifiers. The accumulated loop loss is measured to be approximately 15.5 dB.

At the receiver, the optical signal is pre-amplified and filtered into two separate wavelengths by a WSS. Each wavelength is then fed into a polarization-diverse 90°-hybrid with an independent $\leq$100 kHz linewidth laser as a local oscillator. The electrical signals from the hybrids are sampled using an 8-bit resolution real-time oscilloscope at 80 Gsamples/s and processed offline to compensate for the channel and transceiver impairments.

The offline digital processing is based on [49]. For each wavelength and measurement batch, front-end compensation is performed followed by matched filtering. Then, frequency offset compensation, adaptive equalization and polarization demultiplexing, and carrier phase recovery are applied based on pilot symbols. For the 4QAM payload, a non-data-aided adaptive filter and blind phase recovery algorithm are used. Finally, for VCs, the 2D symbols from physical dimensions are combined together to generate multidimensional symbols, and based on Algorithm 2 in [25], the BER is calculated and averaged over independent symbols realized over the optical channel. For QAM formats, maximum-likelihood detection is applied. In Fig. 5 (b), we show an example of the measured SNR at the receiver for different noise-loaded OSNR values in the B2B measurement for 16QAM. This shows that IQ components experience different implementation penalties in the setup. Therefore, VCs can have different noise distributions between dimensions when they are physically realized over polarizations and wavelengths. This might result in a suboptimal demodulation algorithm in [25].

In Fig. 6, we show the BER performance of a B2B system by sweeping the VOA before the loop-switch and changing the received OSNR. Each VC is compared in different physical realizations with the QAM format at the same SE. Based on Fig. 6, all investigated physical realizations for all VCs show similar performance with negligible deviations which are due to measurement errors. This result indicates that, on average, the B2B channel statistics does not affect the performance of VCs regardless of whether the physical realizations are dependent on each other in different physical realizations or not.

Comparing the AWGN simulation results in Fig. 2 and the B2B experiments in Fig. 6, the implementation penalties for 4QAM and 16QAM formats are 0.7 and 2.7 dB at the HD-FEC limit, respectively. For VCs, the implementation penalties are 0.8, 0.6, and 0.9 dB at $\beta = 1$ bits/sym/dimension, and 2.7, 2.8, and 2.3 dB at $\beta = 2$ bits/sym/dimension for E8, BW16, and BW32, respectively. Due to higher peak-to-average power ratio for VCs, we expect a larger implementation penalty compared to QAM formats. However, with the optical power after each IQ modulator depending on the symbol pattern loaded to the AWG, the measured OSNR based on the total

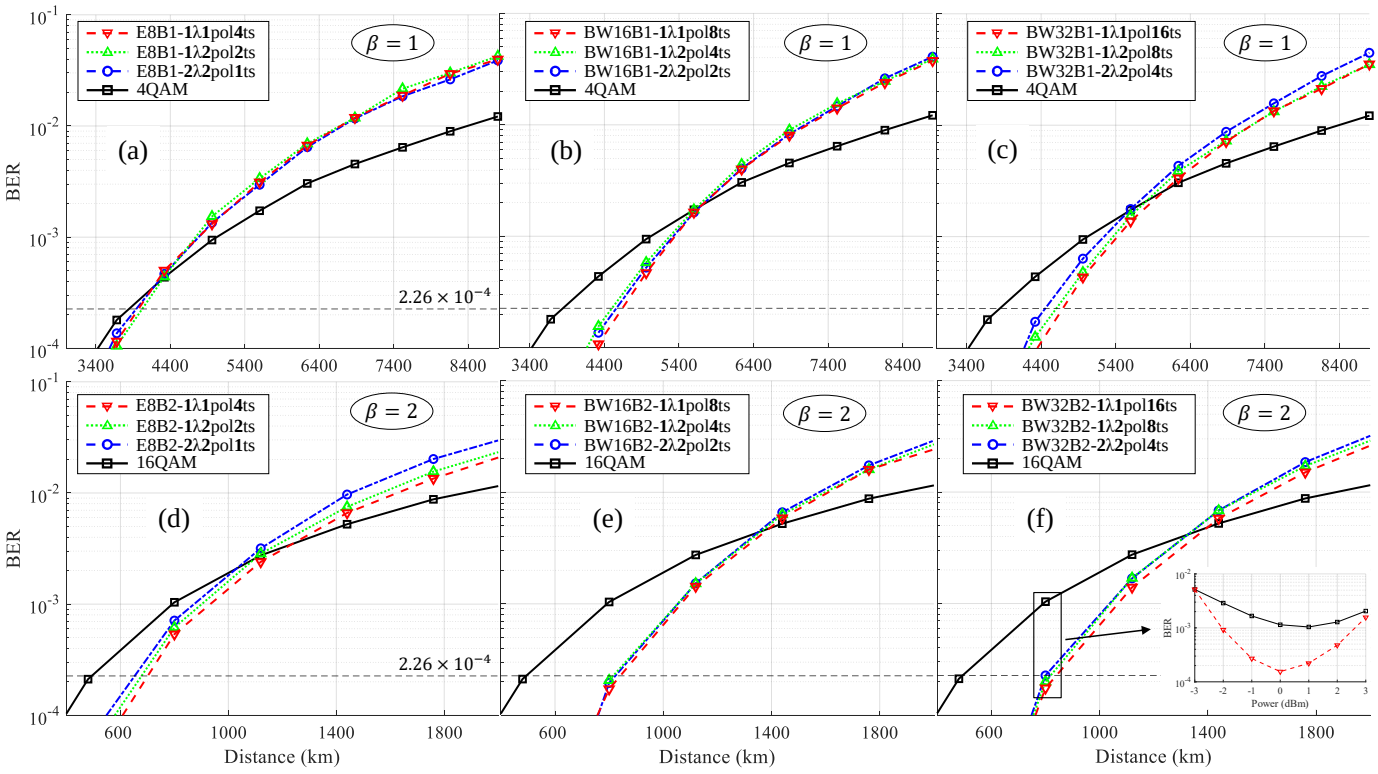

Fig. 7: Experimental BER performance of VCs with different physical realizations and QAM formats using the recirculating loop at the optimum optical launch power. The inset shows BER vs. optical power at a specific transmission distance.

received power might not be accurate for all the channels. Therefore, the measurements have a higher variance for the VCs.

In Fig. 7, we show the BER performance of the VCs and QAM formats in long-haul transmission experiments using a recirculating loop. Each measurement point is optimized by sweeping the total optical power into the fiber from -3 to $+3$ dBm with 1 dB step size. Based on our measurements and simulations, the optimum power is approximately 1 dB lower for VCs compared to QAM formats. Similar to the long-haul simulation results in Fig. 3, expanding the symbol dimensions over time slots and using independent VCs to occupy the available physical dimensions provide an improved transmission reach of up to approximately 4% in Fig. 7 (c) and (d). Furthermore, comparing the performance of VCs with QAM, at the HD-FEC limit of $BER = 2.26 \times 10^{-4}$, the transmission distance improvements are approximately 4.6, 21.4, and 21.9% at $\beta = 1$ bits/sym/dimension, and 42.1, 69.1, and 69.9% at $\beta = 2$ bits/sym/dimension for E8, BW16, and BW32, respectively.

The reason for lower transmission reach in experiments compared to simulations is the component losses in the recirculating loop, including the waveshaper, loop switch, 3 dB coupler, and the noise figure of the amplifier used to compensate for these losses. The performance difference between physical realizations is more evident in experiments compared to simulations, which might be due to the transceiver and loop impairments.

V. Conclusion

In this paper, the performance of different VCs in 8, 16, and 32 dimensions are compared to QAM formats. We showed that VCs outperform QAM formats at relatively high SNRs and low transmission distances. Up to 4.6, 21.4, and 21.9% at 1 bits/sym/dimension and 42.1, 69.1, and 69.9% at 2 bits/sym/dimension transmission reach improvements are shown for 8, 16, and 32-dimensional VCs over QAM formats at the HD-FEC limit. Furthermore, physical realizations of VCs over single-mode fiber show a slightly higher transmission reach when the constellation dimensions are spread over time slots compared to wavelengths or polarizations. However, over a Gaussian noise channel in both simulation and B2B experiments, different realizations perform similarly. Finally, the MI and GMI results indicate that by designing an MLC scheme or an optimized bit labeling, VCs can potentially outperform QAM formats.

References

[1] O. Jovanovic, M. P. Yankov, F. Da Ros, and D. Zibar, "End-to-end learning of a constellation shape robust to channel condition uncertainties," *Journal of Lightwave Technology*, vol. 40, no. 10, pp. 3316–3324, 2022.

[2] H. Dzieciol, G. Liga, E. Sillekens, P. Bayvel, and D. Lavery, "Geometric shaping of 2-D constellations in the presence of laser phase noise," *Journal of Lightwave Technology*, vol. 39, no. 2, pp. 481–490, 2021.

[3] A. Rode, B. Geiger, and L. Schmalen, "Geometric constellation shaping for phase-noise channels using a differentiable blind phase search," in *Optical Fiber Communications Conference (OFC)*, 2022.

[4] G. Liga, B. Chen, and A. Alvarado, "Model-aided geometrical shaping of dual-polarization 4D formats in the nonlinear fiber channel," in *Optical Fiber Communications Conference and Exhibition (OFC)*, 2022.

[5] R. T. Jones, T. A. Eriksson, M. P. Yankov, and D. Zibar, "Deep learning of geometric constellation shaping including fiber nonlinearities," in *European Conference on Optical Communication (ECOC)*, 2018.

[6] D. Pilori, A. Nespola, F. Forghieri, and G. Bosco, "Non-linear phase noise mitigation over systems using constellation shaping," *Journal of Lightwave Technology*, vol. 37, no. 14, pp. 3475–3482, 2019.

[7] B. M. Oliveira, M. S. Neves, F. P. Guiomar, M. C. R. Medeiros, and P. P. Monteiro, "Autoencoder-optimized geometric constellation shaping for unamplified coherent optical links," in *Conference on Lasers and Electro-Optics (CLEO)*, 2022.

[8] E. Agrell and A. Alvarado, "Signal shaping for BICM at low SNR," *IEEE Transactions on Information Theory*, vol. 59, no. 4, pp. 2396–2410, 2013.

[9] J. Cho and P. J. Winzer, "Probabilistic constellation shaping for optical fiber communications," *Journal of Lightwave Technology*, vol. 37, no. 6, pp. 1590–1607, 2019.

[10] T. Fehenberger, A. Alvarado, G. Böcherer, and N. Hanik, "On probabilistic shaping of quadrature amplitude modulation for the nonlinear fiber channel," *Journal of Lightwave Technology*, vol. 34, no. 21, pp. 5063–5073, 2016.

[11] G. D. Forney, Jr., R. G. Gallager, G. R. Lang, F. M. Longstaff, and S. U. Qureshi, "Efficient modulation for band-limited channels," *IEEE Journal on Selected Areas in Communications*, vol. 2, no. 5, pp. 632–647, 1984.

[12] R. F. Fischer, *Precoding and Signal Shaping for Digital Transmission*. John Wiley & Sons, 2005.

[13] Z. Qu, I. B. Djordjevic, and J. Anderson, "Two-dimensional constellation shaping in fiber-optic communications," *Applied Sciences*, vol. 9, no. 9, p. 1889, 2019.

[14] R. T. Jones, M. P. Yankov, and D. Zibar, "End-to-end learning for GMI optimized geometric constellation shape," in *European Conference on Optical Communication (ECOC)*, 2019.

[15] B. Chen, Y. Lei, G. Liga, Z. Liang, W. Ling, X. Xue, and A. Alvarado, "Geometrically-shaped multi-dimensional modulation formats in coherent optical transmission systems," *arXiv:2207.01152*, 2022.

[16] E. Agrell and M. Karlsson, "Power-efficient modulation formats in coherent transmission systems," *Journal of Lightwave Technology*, vol. 27, no. 22, pp. 5115–5126, 2009.

[17] T. A. Eriksson, P. Johannisson, M. Sjödin, E. Agrell, P. A. Andrekson, and M. Karlsson, "Frequency and polarization switched QPSK," in *European Conference on Optical Communication (ECOC)*, 2013.

[18] D. S. Millar, T. Koike-Akino, R. Maher, D. Lavery, M. Paskov, K. Kojima, K. Parsons, B. C. Thomsen, S. J. Savory, and P. Bayvel, "Experimental demonstration of 24-dimensional extended Golay coded modulation with LDPC," in *Optical Fiber Communication Conference (OFC)*, 2014.

[19] E. Sillekens, G. Liga, D. Lavery, P. Bayvel, and R. I. Killey, "High-cardinality geometrical constellation shaping for the nonlinear fibre channel," *arXiv:2205.04391*, 2022.

[20] B. Chen, A. Alvarado, S. van der Heide, M. van den Hout, H. Hafermann, and C. Okonkwo, "Analysis and experimental demonstration of orthant-symmetric four-dimensional 7 bit/4D-sym modulation for optical fiber communication," *Journal of Lightwave Technology*, vol. 39, no. 9, pp. 2737–2753, 2021.

[21] B. Chen, W. Ling, Y. C. Gültekin, Y. Lei, C. Okonkwo, and A. Alvarado, "Low-complexity geometrical shaping for 4D modulation formats via amplitude coding," *IEEE Photonics Technology Letters*, vol. 33, no. 24, pp. 1419–1422, 2021.

[22] J. Conway and N. Sloane, "Fast quantizing and decoding and algorithms for lattice quantizers and codes," *IEEE Transactions on Information Theory*, vol. 28, no. 2, pp. 227–232, 1982.

[23] ——, "A fast encoding method for lattice codes and quantizers," *IEEE Transactions on Information Theory*, vol. 29, no. 6, pp. 820–824, 1983.

[24] G. D. Forney, Jr. and L.-F. Wei, "Multidimensional constellations—part I: Introduction, figures of merit, and generalized cross constellations," *IEEE Journal on Selected Areas in Communications*, vol. 7, no. 6, pp. 877–892, 1989.

[25] A. Mirani, E. Agrell, and M. Karlsson, "Low-complexity geometric shaping," *Journal of Lightwave Technology*, vol. 39, no. 2, pp. 363–371, 2020.

[26] ——, "Lattice-based geometric shaping," in *European Conference on Optical Communications (ECOC)*, 2020.

[27] A. Mirani, K. Vijayan, S. Li, Z. He, J. Schröder, P. Andrekson, E. Agrell, and M. Karlsson, "Comparison of physical realizations of multidimensional Voronoi constellations in single mode fibers," in *European Conference on Optical Communication (ECOC)*, 2022.

[28] A. Mirani, K. Vijayan, Z. He, S. Li, E. Agrell, J. Schröder, P. Andrekson, and M. Karlsson, "Experimental demonstration of 8-dimensional Voronoi constellations with 65,536 and 16,777,216 symbols," in *European Conference on Optical Communication (ECOC)*, 2021.

[29] S. Li, A. Mirani, M. Karlsson, and E. Agrell, "Power-efficient Voronoi constellations for fiber-optic communication systems," *Journal of Lightwave Technology*, 2022.

[30] M. Karlsson, "Four-dimensional rotations in coherent optical communications," *Journal of Lightwave Technology*, vol. 32, no. 6, pp. 1246–1257, 2014.

[31] G. Björk, K. Stensson, and M. Karlsson, "Proposed implementation of "non-physical" four-dimensional polarization rotations," *Journal of Lightwave Technology*, vol. 34, no. 14, pp. 3317–3322, 2016.

[32] J. H. Conway and N. J. A. Sloane, *Sphere Packings, Lattices and Groups*, 3rd ed. Springer, 1999.

[33] S. Li, A. Mirani, M. Karlsson, and E. Agrell, "Low-complexity Voronoi shaping for the Gaussian channel," *IEEE Transactions on Communications*, vol. 70, no. 2, pp. 865–873, 2022.

[34] R.-J. Essiambre, R. Ryf, S. van der Heide, J. I. Bonetti, H. Huang, M. Kodialam, F. J. García-Gómez, E. C. Burrows, J. C. Alvarado-Zacarias, R. Amezcua-Correa *et al.*, "First transmission of a 12D format across three coupled spatial modes of a 3-core coupled-core fiber at 4 bits/s/Hz," in *Optical Fiber Communications Conference (OFC)*, 2020.

[35] D. S. Millar, T. Koike-Akino, S. Ö. Arık, K. Kojima, K. Parsons, T. Yoshida, and T. Sugihara, "High-dimensional modulation for coherent optical communications systems," *Optics Express*, vol. 22, no. 7, pp. 8798–8812, 2014.

[36] M. Mazur, J. Schröder, A. Lorences-Riesgo, T. Yoshida, M. Karlsson, and P. A. Andrekson, "Overhead-optimization of pilot-based digital signal processing for flexible high spectral efficiency transmission," *Opt. Express*, vol. 27, no. 17, pp. 24 654–24 669, 2019.

[37] Y. Wakayama, T. Gerard, E. Sillekens, L. Galdino, D. Lavery, R. I. Killey, and P. Bayvel, "2048-QAM transmission at 15 GBd over 100 km using geometric constellation shaping," *Opt. Express*, vol. 29, no. 12, pp. 18 743–18 759, 2021.

[38] P. Johannisson, M. Sjödin, M. Karlsson, H. Wymeersch, E. Agrell, and P. A. Andrekson, "Modified constant modulus algorithm for polarization-switched QPSK," *Optics Express*, vol. 19, no. 8, pp. 7734–7741, 2011.

[39] M. Sjödin, P. Johannisson, J. Li, E. Agrell, P. A. Andrekson, and M. Karlsson, "Comparison of 128-SP-QAM with PM-16-QAM," *Optics Express*, vol. 20, no. 8, pp. 8356–8366, 2012.

[40] E. Agrell and M. Secondini, "Information-theoretic tools for optical communications engineers," in *IEEE Photonics Conference (IPC)*, 2018.

[41] P. K. A. Wai, C. R. Menyuk, and H. H. Chen, "Stability of solitons in randomly varying birefringent fibers," *Opt. Lett.*, vol. 16, no. 16, pp. 1231–1233, 1991.

[42] G. P. Agrawal, *Nonlinear Fiber Optics*, 5th ed. Springer, 2013.

[43] K. Kojima, K. Parsons, T. Koike-Akino, and D. S. Millar, "Mapping options of 4D constant modulus format for multi-subcarrier modulation," in *Conference on Lasers and Electro-Optics (CLEO)*, 2018.

[44] K. Kojima, T. Yoshida, K. Parsons, T. Koike-Akino, D. S. Millar, and K. Matsuda, "Comparison of nonlinearity tolerance of modulation formats for subcarrier modulation," in *Optical Fiber Communications Conference (OFC)*, 2018.

[45] A. Alvarado, E. Agrell, D. Lavery, R. Maher, and P. Bayvel, "Replacing the soft-decision FEC limit paradigm in the design of optical communication systems," *Journal of Lightwave Technology*, vol. 33, no. 20, pp. 4338–4352, 2015.

[46] S. Li, A. Mirani, M. Karlsson, and E. Agrell, "Designing Voronoi constellations to minimize bit error rate," in *International Symposium on Information Theory (ISIT)*, 2021, pp. 1017–1022.

[47] A. Alvarado, T. Fehenberger, B. Chen, and F. M. Willems, "Achievable information rates for fiber optics: Applications and computations," *Journal of Lightwave Technology*, vol. 36, no. 2, pp. 424–439, 2018.

[48] E. Agrell and A. Alvarado, "Optimal alphabets and binary labelings for BICM at low SNR," *IEEE Transactions on Information Theory*, vol. 57, no. 10, pp. 6650–6672, 2011.

[49] J. Schröder and M. Mazur, "QAMPy a DSP chain for optical communications," 2018. [Online]. Available: github.com/ChalmersPhotonicsLab/QAMpy